International Journal of Automotive and Mechanical Engineering
ISSN: 2229-8649 (Print); ISSN: 2180-1606 (Online);
Volume 14, Issue 3 pp. 4542-4560 September 2017

DOI: https://doi.org/10.15282/ijame.14.3.2017.12.0359

Investigation of thermal-hydraulic performance in flat tube heat exchangers at various tube inclination angles

A. Y. Adam*, A. N. Oumer, Azri Alias, M. Ishak and M. M. Noor

Faculty of Mechanical Engineering, Universiti Malaysia Pahang,
26600 Pekan, Pahang, Malaysia,
*Email: ahmnur99@gmail.com

ABSTRACT

The performance of compact fin-and-flat tube heat exchangers (HE) can be affected by many geometrical and processing factors and one of them is tube inclination angle. However, the effect of flat tube inclination angle on the thermal-hydraulic performance of the HE is not fully examined. This paper investigates the effects of flat tube inclination angles on heat transfer and pressure drop characteristics of fined flat tube HE when the tubes are deployed in in-line and staggered arrangements. A symmetric numerical method based on FLUENT software was carried out with six different tube inclination angles (0°, 30°, 60°, 90°, 120°, and 150°) in moderately high Reynolds number. From the results, it was observed that heat transfer coefficient increased with the augmentation of the tube inclination angle from 0^o to 90^o and decreased for 120^o and 150^o. With the increase of tube inclination angle, the average Nusselt number rose by 36.3%. This might be due to the reason that the tube surface area increases with the inclination angle, which also results in the largest increment of the pressure drop by 42.0%. Overall, the 90^o tube inclination angle showed the highest enhancement in heat transfer for both inline and staggered configurations with a maximum enhancement of 41.2% for in-line and 32.2% for staggered arrangements. However, the heat transfer enhancements were accompanied by high-pressure drop penalties of up to 44.2% and 42.6% for in-line and staggered arrangements, respectively. Therefore, inclining the tubes at 90^o is recommended where high heat transfer is required. On the other hand, 0^o tube inclination angle is recommended where pumping power is a crucial issue.

Keywords: Numerical methods; heat exchangers; heat transfer; pressure drop; turbulent flow

INTRODUCTION

In many industrial and engineering applications, high thermal efficiency and economic competitiveness can be achieved by heat exchangers (HE) with special thermal properties, better flow, and heat characters. The performance of a HE affects the effectiveness of the heat exchange and this makes HE an important issue in studies of energy saving [1]. Since global energy consumption is negatively affecting the environment and causing ozone depletion, an increasingly more intelligent use of the available energy is required. As a result, the increased competitiveness of the manufacturing cost becomes a significant issue. Thus, all manufacturers are trying to design HE with high energy efficiency and lower manufacturing costs. Consequently, there are a large number of scientific research in recent times on the maximisation of the utilisation of the available energy [2, 3], and

enhancement of air-side heat transfer performances. Among the many types of HE in recent years, performance improvements in its compact designs have become a common engineering topic. Compact HE has been widely used in many industrial applications due to its compactness, low weight, high competence and low cost. It includes two sorts of HE either fin-and-tube or plate-and-fin [4-8]. Fin and tube HE, in particular, has been used in engineering fields such as chemical engineering, petrochemical, heating ventilation and air conditioning, compressors, and fan coils. Moreover, they play important role in electronics cooling. Compact HE has substantial small sizes due to the reason that the highest thermal resistance occurs in the air side of the HE compared to the tube side and wall conductive thermal resistance, which makes the air side heat transfer coefficient relatively small [4, 9-11]. Hence, to decrease the size of HE, significant improvements have been employed on the air side. As the dominant air side thermal resistance can reach up to 90% of the total thermal resistance, researchers have devoted their effort to enhance the heat transfer process by attaching fins on the tube surface which augments the heat transfer rate by increasing the heat transfer surface area [12, 13]. Moreover, the pressure drop penalty associated with attaching the fins has been given attention. Therefore, the current challenge faced by the researchers is to improve the fin geometry in order to enhance the transfer of heat associated with the low-pressure drop across HE.

In general, the thermal hydraulic diameter of flat tube HE is smaller than that of circular tubes of the same cross-sectional area [14]. Using circular tubes in HE has many drawbacks such as high drag on the tube and low heat transfer on the fin behind the tubes due to the fact that the flow accelerates around the heated tube and forms a low-velocity wake region behind the tubes. Thus, the heat transfer coefficient of the fin is not uniform and depends on the fin position. These drawbacks can be overcome by using either oval or flat tube. Compared to round tube HE, flat tube HE has better air-side heat transfer coefficient and lower pressure drop due to small wake area behind the tubes [15]. Moreover, noise and vibration levels in flat tubes are expected to be lower than that of circular tubes [16, 17]. The performance of compact HE can be affected by many geometrical and processing factors. Some of the factors include tube and fin material, tube shape, tube spacing, tube inclination angle, fin spacing, and fin type. Some researchers have studied the effects of some of the aforementioned parameters on the thermal-hydraulic performance of flat tube HE. Numerous numerical and experimental studies have been done to determine the air-side thermal and flow performances using different types of tubes and fins [10, 18-22]. Nascimento and Garcia [23] reported that flat tube with a shallow square dimple enhanced the heat transfer considerably. More recently, Duan et al. [24] revealed that longitudinal and transversal vortices can be created by using intermittent wavy fins with the flat tube HE and producing great heat transfer enhancement. P. Wais [25] performed a three-dimensional simulation using ANSYS software with fixed inlet air velocity and fin spacing to analyse the effect of louver inclination angle of a car radiator having circular tubes. They found that heat transfer depends strongly on the louver angle and the maximum value of the outlet air temperature reaches at 45º. Generally, the performance of the HE can be affected by the variation of the geometrical parameters as documented in early experimental works by E. Sparrow and F. Samie [26]. They studied the influence of the number of tube rows and revealed that for one–row arrays, the Nusselt number increases with the decreasing tube transverse pitch. Furthermore, J. Dong et al. [27] experimentally investigated the effects of fin pitch on multi-louvered flat tube HE using 20 types of HE having different fin pitches. More recently, P. Wais [25] performed a three-dimensional simulation using ANSYS software

with fixed inlet air velocity and fin spacing to analyse the effect of louver inclination angle of a car radiator having circular tubes. The heat transfer strongly depends on the louver angle and the maximum value of the outlet air temperature reaches at 45º louver inclination angle. In another study, L. Yang et al. [28] numerically investigated the effect of fin height on the performance of HE with wavy fins and flat tubes. Their results showed that the Nusselt number (Nu) increased slightly with the increasing fin height, particularly at low Reynolds number. However, to the best of the authors' knowledge, the effect of flat tube inclination angle on the thermal-hydraulic performance of fin-and-tube HE has not been fully examined. Thus, an extensive study focusing on the performance of finned and flat tube HE with the inclined flat tube is necessary.

This paper aims to investigate the effect of tube inclination angle on the thermal and hydraulic performance of fined flat tube HE when the tubes are deployed in an in-line and staggered three by three rows of arrays. A symmetric numerical method based on Ansys FLUENT software was carried out with six different tube inclination angles (0°, 30°, 60°, 90°, 120°, and 150°) in moderately high Reynolds number. The standard k–ε model was used due to the fact that it is a widely used turbulence model for the solution of practical engineering flow problems. The findings of this study could help engineers in their decision at an angle should the tubes be inclined against the incoming air when designing compact HE for enhanced heat transfer and reduced pressure drop. Moreover, manufacturers who are trying to design HE with high energy efficiency might also benefit from this research work.

METHODS AND MATERIALS

Problem Description

The schematic diagrams of cross-sections of the fin-and-tube compact HE with in-line and staggered configurations considered in this study are shown in Figure 1. Air flowed across the fin and tube surfaces while constant heat flux was supplied from the tube inner surfaces. The physical models consisted of flat tubes with overall length of 220 mm and tube hydraulic diameter of 15.1 mm and square fins with dimensions of 110 mm × 110 mm × 0.6 mm. Other geometrical parameters such as tube transverse pitch (P_t), tube longitudinal pitch (P_l), fin pitch (S), and fin thickness (δ) are presented in Table 1. Moreover, schematic of the six different tube inclination angles against the incoming air considered for this study are shown in Figure 2. Since there is temperature variation through the fluid and the solid domains due to thermal interactions, such kind of heat transfer is known as conjugate heat transfer. Conjugate heat transfer has the ability to couple the heat transfer by conduction through solid domain while the heat transfer by forced convection [4, 29]. The computational domains for a three-row by three-column in-line and staggered fin-and-tube HE considered for the numerical analysis are shown in Figure 3. Due to the symmetry nature of the geometries, the sections represented by the dashed lines in Figure 3 are selected as computational domains. Moreover, the computational domains are extended by one time tube transverse pitch (P_t) in the upstream side to ensure that there is no flow disturbance and the velocity profiles are uniform when they reach the fin and tube surfaces. In addition, the domains are extended six times the tube transverse pitch at the downstream to ensure that the outflow can be applied at the outlet and prevent flow recirculation [30]. Thus, the selected computational domains are seven times the actual heat transfer areas.

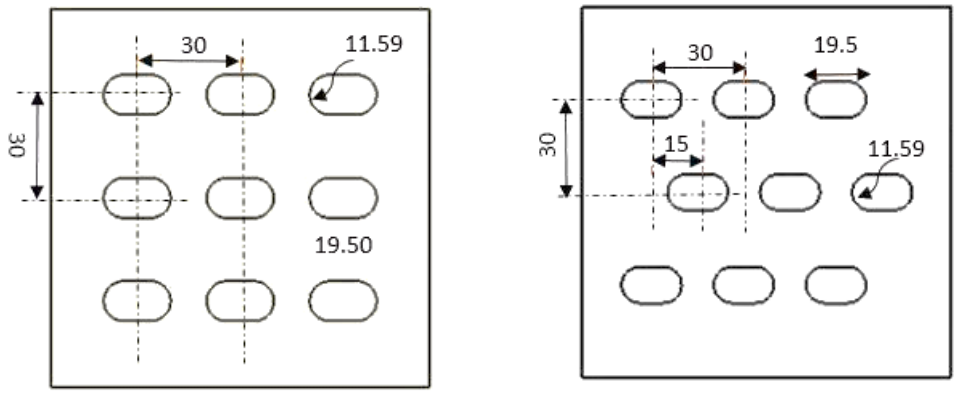

(a) (b)

Figure 1. Schematic diagrams of cross-sections of fin-and-tube HE with (a) in-line and (b) staggered arrangements (all dimensions are in mm).

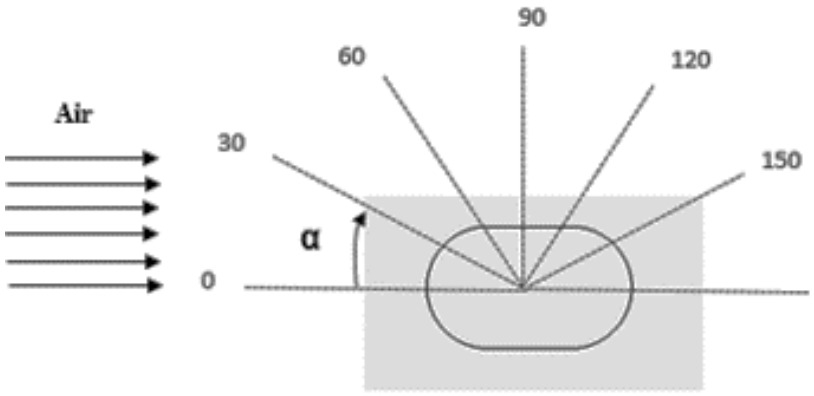

Figure 2. Angles of attack for the flat tube against the incoming air.

Table 1. Computational domain geometric details.

Name	Value (mm)	Symbol
Tube transverse pitch	30	P_t
Tube longitudinal pitch	30	P_l
Tube outside diameter	11.59	D_o
Tube hydraulic diameter	15.1	D_h
Fin thickness	0.6	δ
Fin spacing	20	S
Tube and fin material	-	Aluminium (al)

Mathematical Formulation

Governing Equations

The mathematical formulation is based on the assumptions that the flow field is incompressible, turbulent, non-isothermal, and steady. Moreover, the physical properties are assumed to be constant, the thermal radiation and heat dissipation are neglected, and the fin surfaces are assumed to be smooth. Based on these assumptions, therefore, the continuity, momentum, and energy governing equations are solved along with the transport equations of the turbulent kinetic energy and its dissipation rate. The continuity, momentum, and energy equations will be in the following form:

$$\nabla.(\boldsymbol{V}) = 0 \tag{1}$$
$$\rho\nabla.(\boldsymbol{VV}) = -\nabla P + \nabla.\tau \tag{2}$$
$$\rho C_p \nabla.(T\boldsymbol{V}) = k\nabla.T \tag{3}$$

where $\boldsymbol{V}$ is the velocity vector, ρ is the density, p is the hydrostatic pressure, τ is the fluid shear stress, and T is the temperature. The terms k and C_P represent the thermal conductivity and constant-pressure of the specific heat.

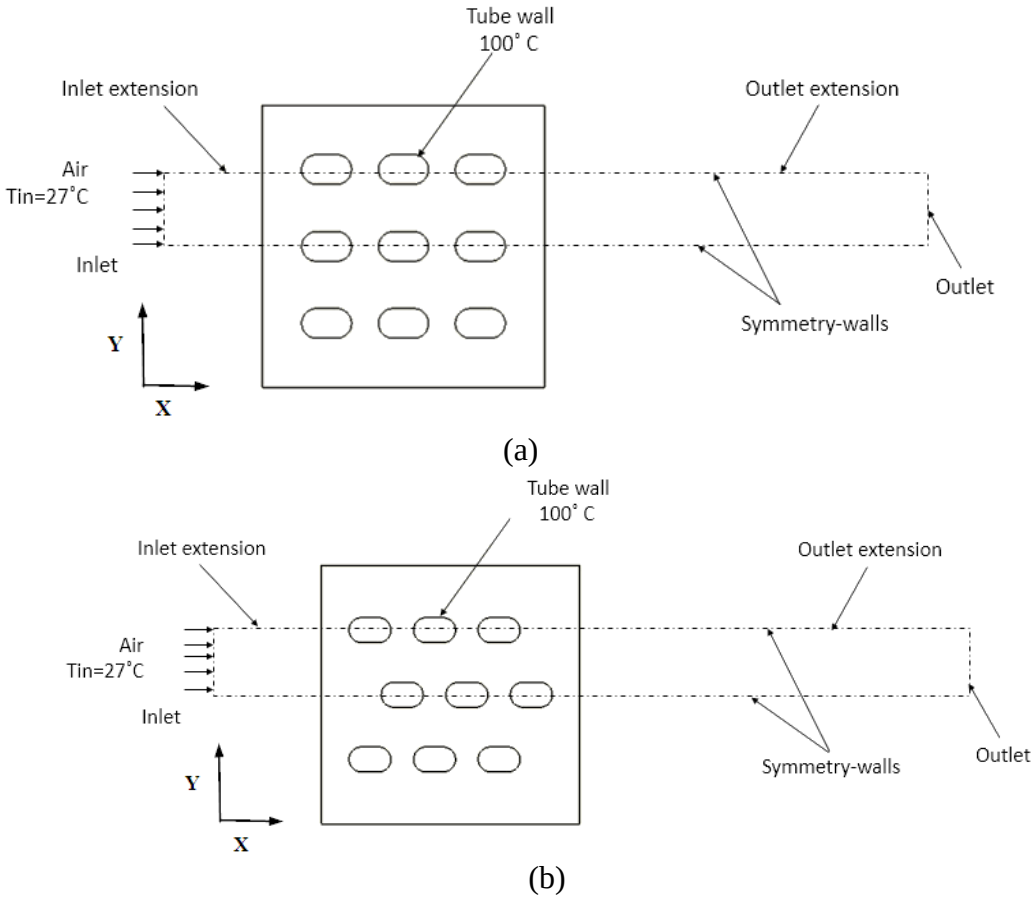

Figure 3. Computational domain for (a) in-line and (b) staggered configurations.

The transport equations for the standard $k-\varepsilon$ model can be written as [31, 32]:

$$\rho\frac{\partial(k\,\mathrm{V})}{\partial X} = \frac{\partial}{\partial X}\left[\left(\mu + \frac{\mu_t}{\sigma_t}\right)\frac{\partial k}{\partial X}\right] + G_k + G_b - \rho\varepsilon - Y_M + S_k \tag{4}$$

$$\rho\frac{\partial(\varepsilon V)}{\partial X} = \frac{\partial}{\partial X}\left[\left(\mu + \frac{\mu_t}{\sigma_\varepsilon}\right)\frac{\partial \varepsilon}{\partial X}\right] + G_{1\varepsilon}\frac{\varepsilon}{k} + \left(G_k + G_{3\varepsilon}G_b\right) - G_{2\varepsilon}\rho\frac{\varepsilon^2}{k} + S_\varepsilon \tag{5}$$

where k, ε, μ, *and* μ_t are the turbulence kinetic energy, rate of dissipation, dynamic viscosity of air, and turbulent (eddy) viscosity, respectively. The term G_k is the generation of turbulent kinetic energy caused by the mean velocity gradient, G_b is the generation of turbulence kinetic energy as a result of the buoyancy, and Y_M denotes the contribution of

the fluctuating dilatation in compressible turbulence to the overall dissipation rate. The turbulent viscosity can be computed as:

$$\mu_t = \rho C_\mu \frac{k^2}{\epsilon} \tag{6}$$

The other parameters, $G_{1\epsilon}, G_2$, σ_k and σ_ϵ are constants and their default values are 1.44, 1.92, 1, and 1.3, respectively.

Parameter Definitions

Heat transfer and pressure drop characteristics for compact HE depend on the conditions of the air flow and geometry of the HE. Thus, the flow and heat transfer parameters namely Reynolds number, Nusselt number, Colburn factor, and friction factor are used to describe the thermal-hydraulic performance of the compact HE. The Reynolds number (*Re*), Colburn factor (*j*), and friction factor (*f*) can be defined using Equation (7), (8), and (9), respectively [30].

$$Re = \frac{\rho u_{max} D_h}{\mu} \tag{7}$$

$$j = \frac{h}{\rho u_{max} C_P} Pr^{\frac{2}{3}} \tag{8}$$

$$f = \frac{D_h}{L} \frac{2\Delta p}{\rho {u_{max}}^2} \tag{9}$$

where, *Pr* is Prandtl number, Δp is the pressure drop, and *L* is the air flow length. The heat transfer coefficient between the finned flat tube and air is determined as:

$$h = \frac{q}{(T_{wall} - T_{mean})} \tag{10}$$

where *h* is the heat transfer coefficient, *q* is the rate of heat flux at the tube wall, T_{wall} is the tube surface wall temperature, and T_{mean} is the free fluid mean temperature at the particular location around the tube. The mean temperature of the air at any particular position of the computational domain can be computed using the following equation [33]:

$$T_{mean} = \frac{\int T \rho \vec{u} \,.\, d\bar{A}}{\int \rho \vec{u} \,.\, d\bar{A}} \tag{11}$$

The average Nu number can be obtained by averaging the values of local heat transfer coefficients for all surfaces involved in the heat transfer:

$$Nu = \frac{h D_h}{k} \tag{12}$$

where D_h and k are the hydraulic diameter and thermal conductivity, respectively.

The boundary conditions used in the computations are shown as follows:

i) Uniform velocity and temperature (300 K) are assigned to the inlet boundary.
ii) No slip conditions are used on all tube walls. Symmetry conditions are assigned to the lateral surfaces of the test section.
iii) The tube wall temperatures are fixed at 373 K.
iv) The computational domain is extended downstream for fully developed outlet boundary condition.
v) Symmetrical boundary conditions are assigned to other surfaces.

Mesh Generation and Independence Test

The Navier-Stokes and energy equations outlined in Equation (1-5) with the corresponding boundary conditions were solved using Fluent 15 computational fluid dynamics software. The heat transfer and airflow over the tube bundles were treated using the standard *K*-ε turbulence module. The mesh around the tube walls was refined with great care in order to provide accurate results. The wall quantities (velocity gradients, pressure, etc.) are very important and the flow separation and reattachment are strongly dependent on an accurate prediction of the turbulence development near the walls. Due to this reason, enhanced wall treatment was selected in Fluent instead of standard wall function. Second-order upwind scheme was used to discretise the convective terms and SIMPLE-algorithm was applied to perform the coupling between the pressure and velocity terms. Absolute convergence criteria were chosen for the velocity and energy parameters with numerical values of 1×10^{-4} and 1×10^{-6} respectively.

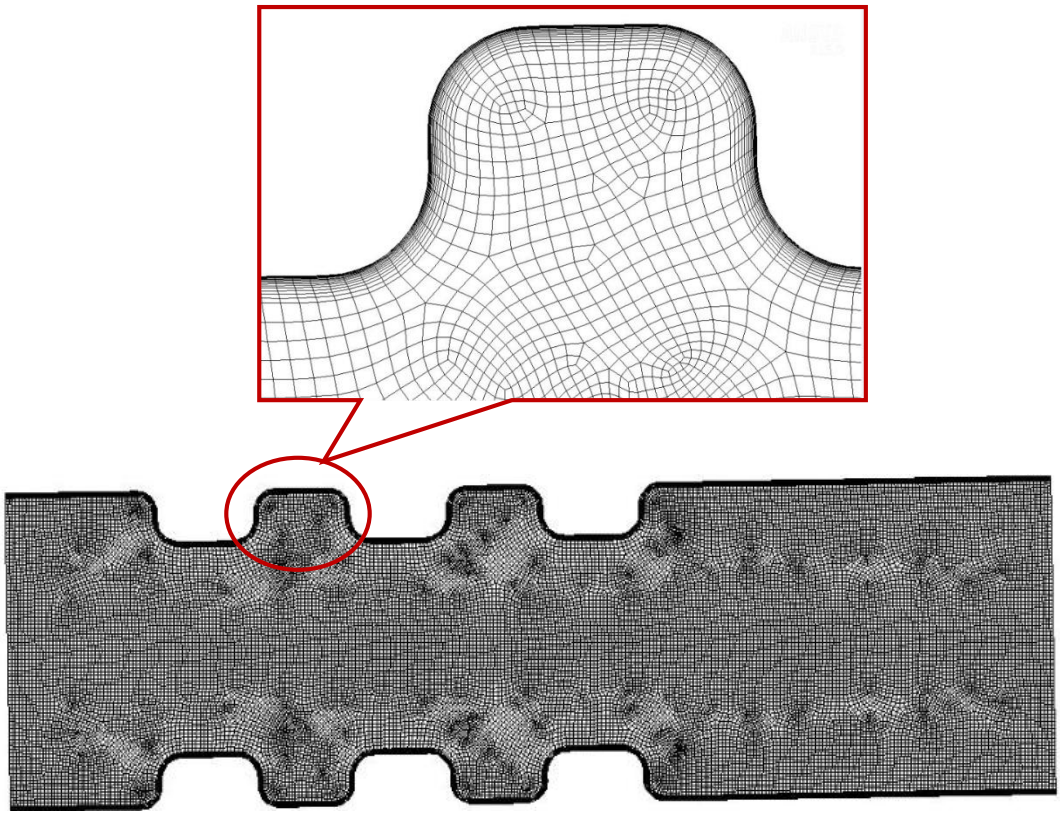

Figure 4. Grid distributions for the computations.

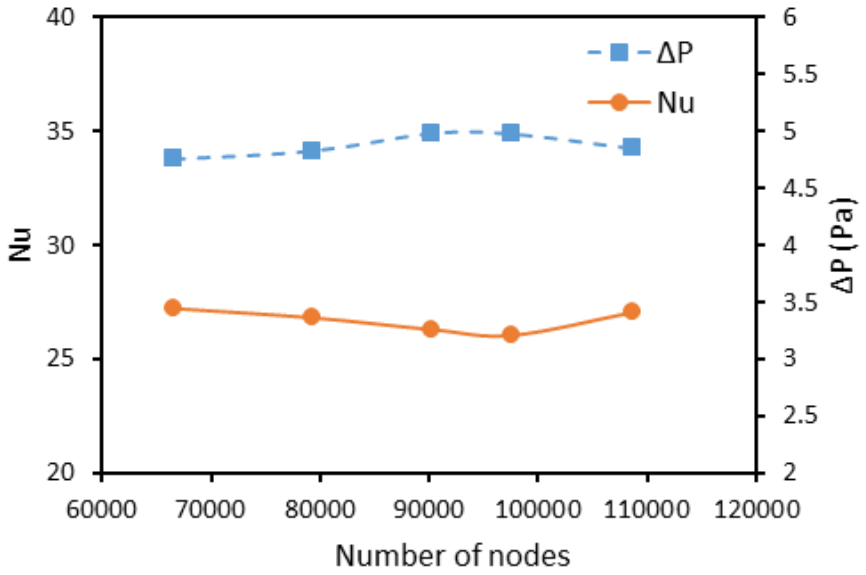

Figure 5. Nusselt number and pressure drop results for zero angle of attack and Re=3500 using different grid sizes.

In this study, the grids were generated with great care. Firstly, the flow domain was divided into three subdomains according to the gradient level at the region. Thereafter, various strategies were employed for the subdomains in order to generate appropriate grid sizes. In order to provide accurate results, the grids around the flat tubes were refined with unstructured quadratic as shown in Figure 4. Prior to conducting the simulations to investigate the effect of tube inclination angle on the performance of heat transfer and pressure drop, it is necessary to examine whether appropriate grid density is adopted. This is to make sure that the relative changes in the velocity and pressure fields are less than 5%. Consequently, a grid independence test was conducted using five different grid sizes, 66550, 79244, 90242, 97634, and 108692 for the case where the tubes inclination angle is zero and Reynolds number is 3500. Figure 5 shows the mesh independency results for the different grid sizes. It was found that the difference in the average Nu number and Δp between 90242 and 97634 grid sizes was 1.79% and 3.08%, respectively, which is less than 5%. Therefore, the final grid size adopted in this study was 90242 to discretise the whole computational domain.

Validation of the Computational Model

To check the reliability of the developed numerical model, the Nu results from the current model were compared against the results of other benchmark studies. Therefore, the results for air-side forced convection in finned circular tube HE obtained from the present model were validated against the benchmark experimental results by Zukauskas [34] and numerical solutions developed by Gholami et al. [35]. The circular tube HE used for the validation was three rows by four columns of tubes with geometrical details where the tube outside diameter was 10.55 mm, transverse pitch was 25.4 mm and the longitudinal pitch was 22 mm. Figure 6 shows a variation of average Nu with Reynolds number. A good agreement can be observed between the results of the present study and the other benchmark results for the Nu. The maximal deviations between the predicted values of Nu number by the present model and the values obtained by Zukauskas [34] experimental data and Gholami et al. [35] numerical solutions were 9.6% and 11.9%, respectively. This shows that the Nu results obtained by the present model are located within the allowable

error range. Therefore, the good agreement between the simulated and published results indicate that the current numerical model is reliable to predict the heat transfer and pressure drop characteristics.

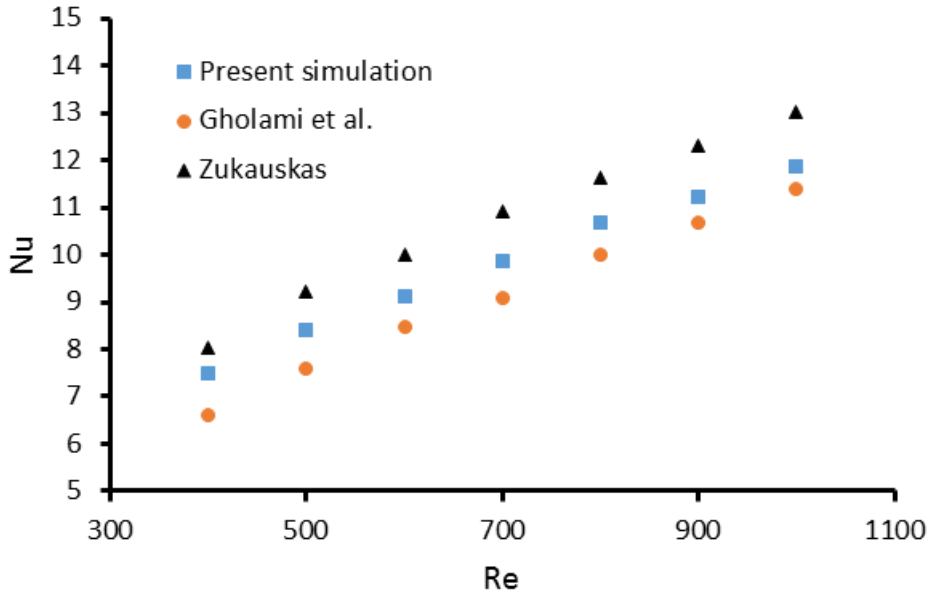

Figure 6. Comparison of the present study simulation to Zukauskas [34] correlation and Gholami et al. [35] simulation.

RESULTS AND DISCUSSION

After successfully validating the numerical model, the next stage is to study the effect of inclination angle ($0^o \le \alpha \le 150^o$) of flat tubes on the forced convection flow structure, heat transfer characteristics, and pressure drop in cross-flow flat tube HE. The analysis was conducted for Reynolds number ranging between 3500 and 7300.

Effect of Tube Inclination Angle on Flow Structure

Figure 7 and 8 are the effects of tube inclination angle on the flow structure for in-line and staggered arrangements, respectively. Both figures show the local velocity distributions for the case where Re = 3500. It can be clearly seen from the figures that there are recirculation zones after each tube for both in-line and staggered configurations as a result of tube blockage which leads to fluid separation. Wherever the flow separates at the back of the tube, it is rebound at the frontal segment of the subsequent tube to constitute a superior region in the middle of two adjacent tubes. Moreover, there are strong swirling flows behind the tubes on the tubes wake area and the swirling strength increases with increasing inclination angle from 0^o to 90^o. Similar results were obtained for elliptical tubes where the effects of the vortex formation and shedding on the velocity and thermal fields were more pronounced in the case when the angle of attack tend to be at a right angle with a lower value of the axis ratio [33]. This was due to the reason that as the angle of attack increases from 0^o to 90^o,the air departs from the first row of tubes as jets, which in turn enhances the degree of turbulence through the flat tube arrays passages, thus forming vortex shedding.

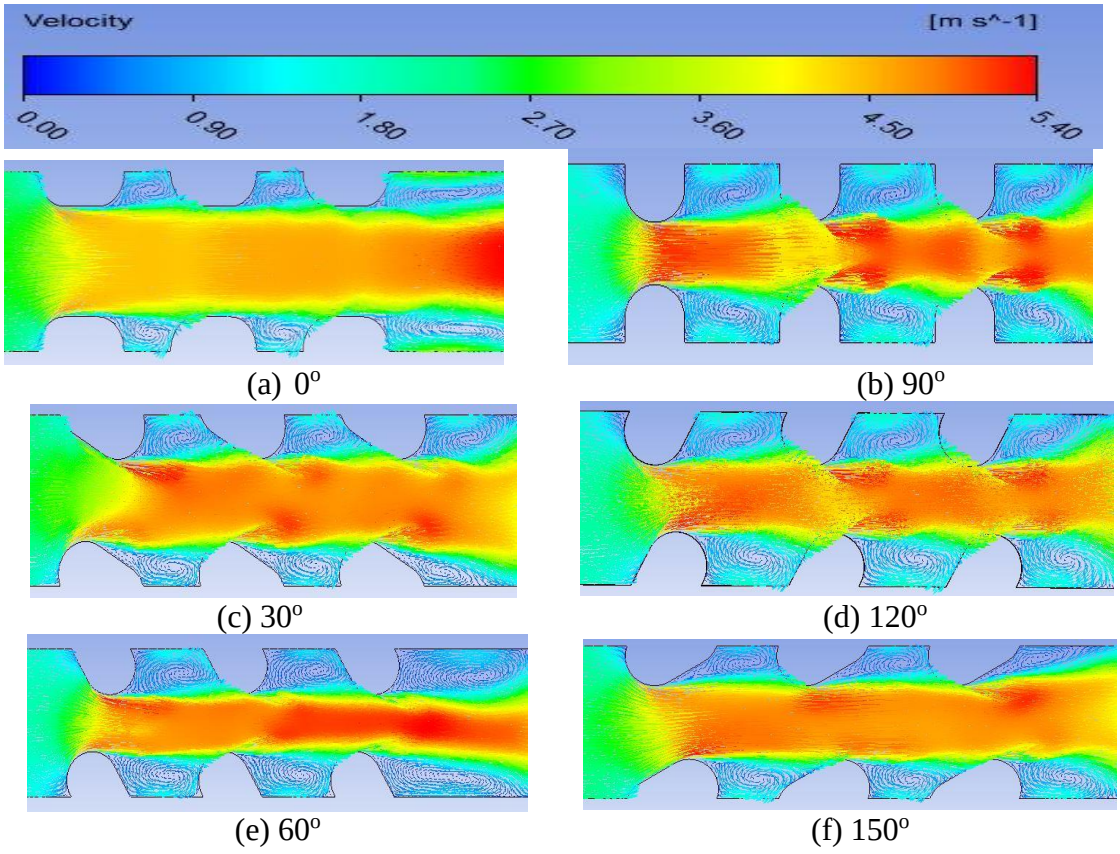

Figure 7. Local velocity distribution for in-line configuration at Re=3500.

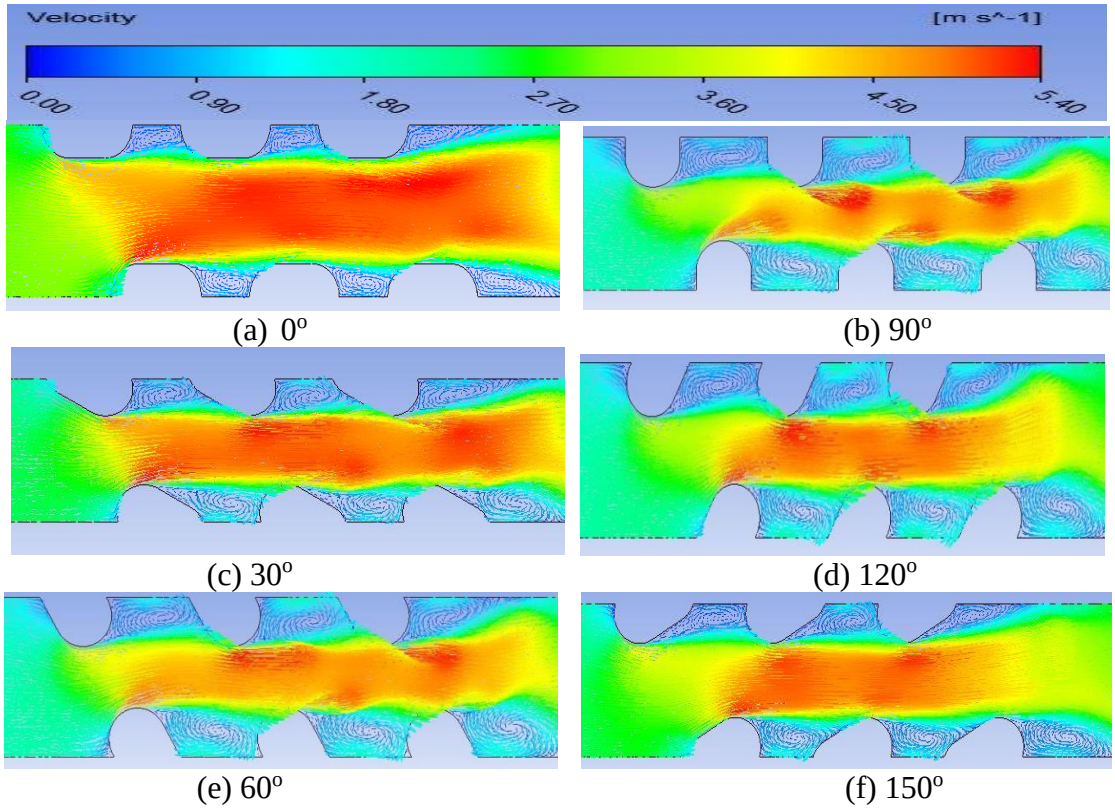

Figure 8. Local velocity distribution for staggered configuration at Re=3500.

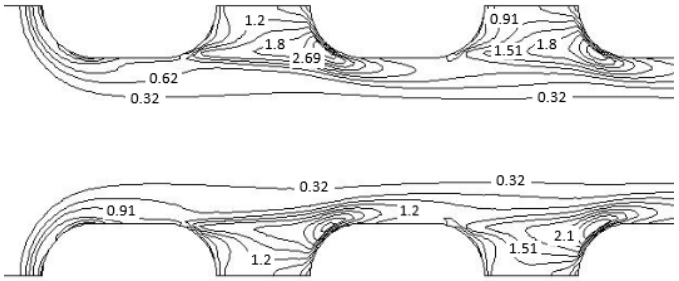

(a) α=0°

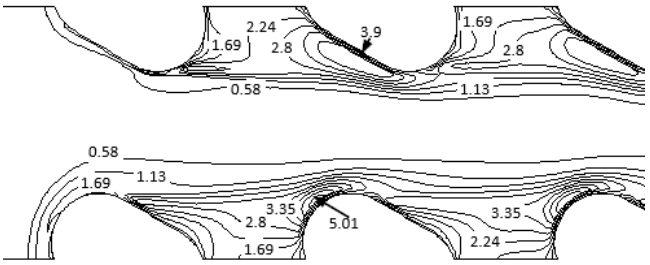

(b) α=30°

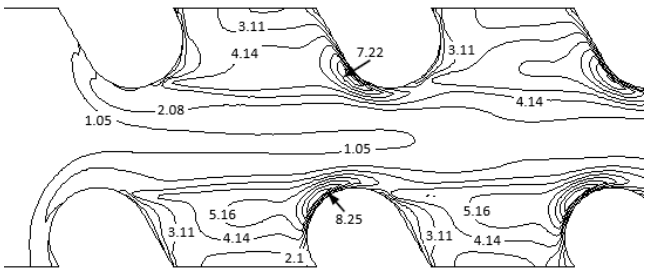

(c) α=60°

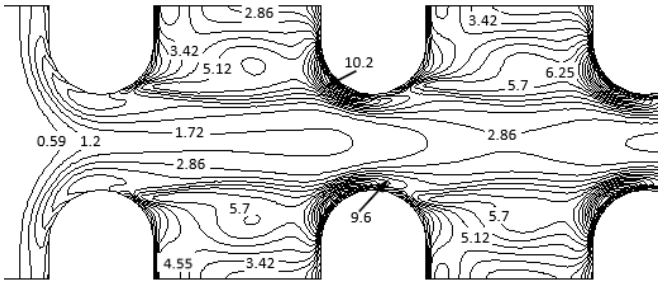

(d) α=90°

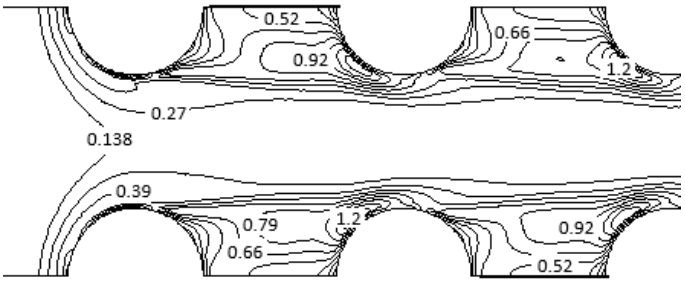

(e) Circular

Figure 9. Contours of turbulent kinetic energy per unit mass for (a) α=0°, (b) α=30°, (c) α=60°, (d) α=90°, and (e) circular at Re=3500.

Nevertheless, for 120^o and 150^o, the swirling intensity reduced as depicted in Figure 7 and 8 for both arrangements. Such strong swirling has a significant effect on the main flow in such a way that it might disturb the growth of the boundary layer on the fin surfaces, drag the fluid from the wake region and enhance the fluid mixing. Therefore, all these will result in a considerable enhancement of the heat transfer. It is obvious from the figures that the velocity magnitude on the rare area of the tubes was very low compared to the front flow. As the angle of inclination increased the momentum behind the tube became higher due to the high swirling, vortices formed which recirculated and compressed the fluid and therefore delayed the flow separation and reduced the tube wake area. For the flat tube with zero inclination angle (α=0°), the drag was found to be less than those obtained with the circular tube. This indicates that flat tubes have better aerodynamics.

Virtually, the unique structure of the flat tubes enhanced the turbulence level and increased the air velocity over the tube banks. However, the intensity of the turbulence is dependent on the velocity of the incoming air and the tube inclination angle. As the air passed over the first row of tube bank the flow intensity increased behind the tubes. Thus, the flow behind the tubes wake area disturbed the development of the thermal boundary layer, which resulted in a considerable enhancement of the heat transfer coefficient. Figure 9 refers to the contours of the turbulent kinetic energy per unit mass for the finned-flat tube HE with tube inclination angles of 0°, 30°, 60°, and 90° and finned-circular tube HE as well. It can be seen from the contours that the turbulent kinetic energy values increased with the increment of tube inclination angle. The highest value of the turbulent kinetic energy was achieved at tube inclination angle α=90°. On the other hand, the lowest value happened with the tube inclination angle α=0°. The turbulent kinetic energy produced by circular tube banks was less than the flat tube banks at all inclination angles.

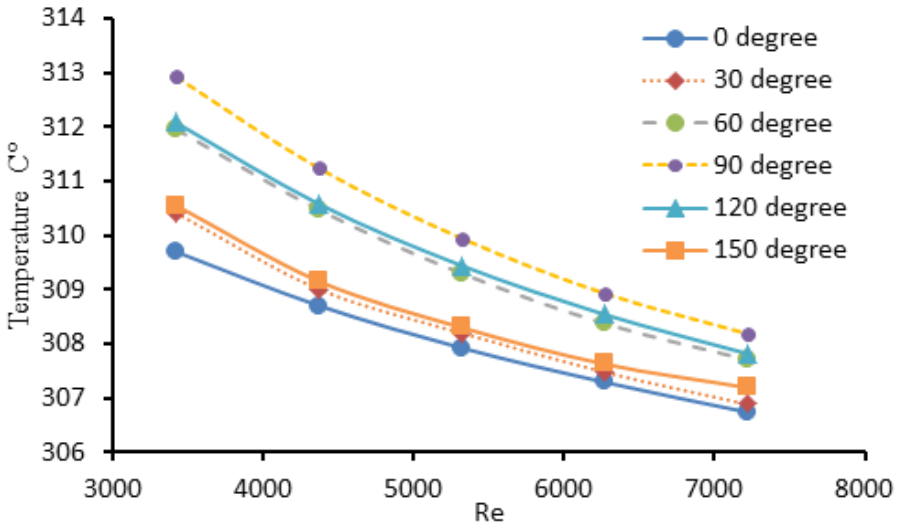

Figure 10. Variation of outlet temperature at various tube inclination angles.

Effect of Tube Inclination Angle on Heat Transfer

The outlet temperature at various tube inclination angles is presented in Figure 10. It can be clearly observed from the figure that the outlet temperature increased with the increasing tube inclination angle. This might be due to the reason that the temperature gradient was very small in the tube wake area at small inclination angles. On the other hand, when the angle of attack increased the temperature gradient was highly augmented

as a result of better mixing that occured in the area behind the tube. Consequently, the flux from the tube surfaces was higher which enhanced the heat transfer in the flow channel. Moreover, the accelerated flow due to better mixing behind the first tube impinged the second tube and resulted in high heat transfer. As expected, the outlet temperature values for the 150^o tube inclination angle were slightly close to those obtained by 30^o. Similar trends of temperature variation for 120^o and 60^o were obtained. The highest outlet temperature was obtained at 90^o tube inclination angle for all Reynolds numbers. Moreover, for all inclination angles, the temperature gained by the air at the outlet became small as the inlet velocity increased. For instance, at 0^o, 90^o, and 150^o tube inclination angles, the temperature gained by the air outflow decreased by0.95%, 1.52%, and 1.08%, respectively, when the Reynolds number at inlet increased from 3417 to 7215. This might be due to the fact that the air molecules will absorb more energy at slow velocities than fast molecules to transfer energy to the wave.

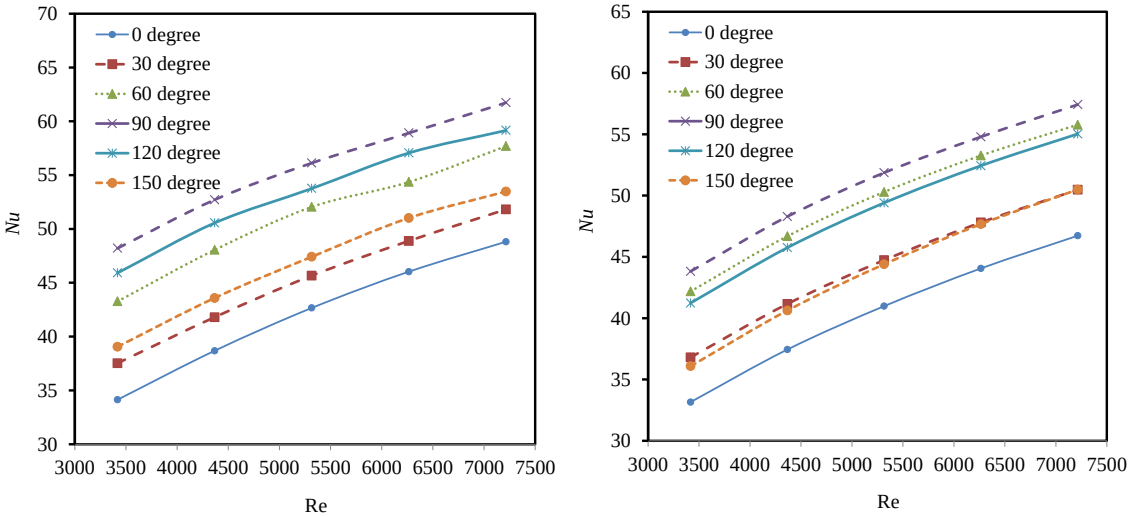

Figure 11. Variation of Nusselt number with Reynolds number for (a) in-line (b) staggered configurations at different inclination angles.

Figure 11 is a variation of the average Nusselt number (Nu) with Reynolds number for both in-line and staggered arrangements at various tube inclination angles. It can be clearly seen from the figure that there is a significant difference between the results of Nu for 0° and other tube inclination angles. In fact, the average Nu increased with the increasing Reynolds number at all angles. As expected, the average Nu values for tube inclination angles of 30° and 60° were close to the values for 120° and 150°, respectively, whilst the 90° inclination angle produced the highest Nu for both in-line and staggered arrangements. For in-line arrangement, considering the 0° inclination angle as reference, the maximum average Nu increments were 9.5%, 26.8%, 41.2%, 34.5%, and 14.4% for 30°, 60°, 90°, 120°, and 150° inclination angles, respectively. Similarly, the maximum Nu increments for staggered arrangement were 11%, 27.2%, 32.2%, 24.2%, and 8.8% for 30°, 60°, 90°, 120°, and 150° inclination angles, respectively. Comparing the Nu of the flat and circular tubes at Re= 3500, the Nu number for the circular tube was higher than that of the flat tubes with tube inclination angles of 0° and 30° by 14.3% and 5.8%, respectively. On the other hand, at 60° and 90 ° tube inclination angles, the Nu number for the circular tube was lower than that obtained by the flat tube by 8.7% and 21%,

respectively. It can also be observed from Figure 11 that the in-line arrangement provided better heat transfer enhancement than the staggered arrangement. This might be due to the reason that the staggered arrangement shows the formation of uneven (unsymmetrical) circulation around the tube walls. In general, for both in-line and staggered arrangements, inclining the flat tubes against the incoming air can increase the Nu. Again, this can be an indication of improved heat transfer performance by increasing the inclination angle of the tubes.

Effects of Tube Inclination Angle on Pressure Drop

Illustrated in Figure 12 are the pressure drop variations for different configurations of flat tube banks at various tube inclination angles. It can be observed from the figure that there is a significant increment in pressure drop when the inclination angle increases from 0^o to 90^o even at low Reynolds number. The maximum pressure drop was registered at 90° inclination angle and Re =7214 for both in-line and staggered arrangements with values of 57.2 Pa and 54.9 Pa, respectively. The high-pressure drop might be due to the reason that the surface area of the tubes that comes in contact with the incoming air is high for 90^o inclination angle causing extra drag to be induced and resulting tube blockage. Therefore, we can conclude that the heat transfer enhancement observed by tilting the tubes by a certain angle is associated with high-pressure drop penalty.

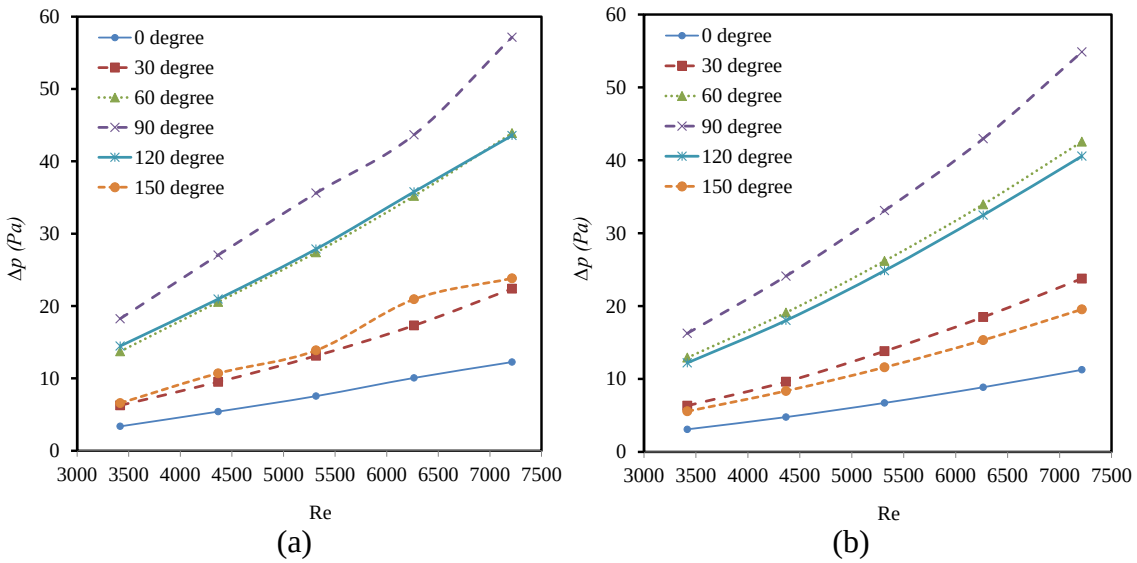

Figure 12. Variation of the pressure drop with different Reynolds number for (a) In-line and (b) staggered arrangements.

Figure 13 and 14 present pressure drop contours for the finned flat tube HE with in-line and staggered configurations at various tube inclination angles. The contours display that the pressure decreased along the tube banks. It can also be noted that staggered configuration provides low-pressure drop compared to in-line arrangement.

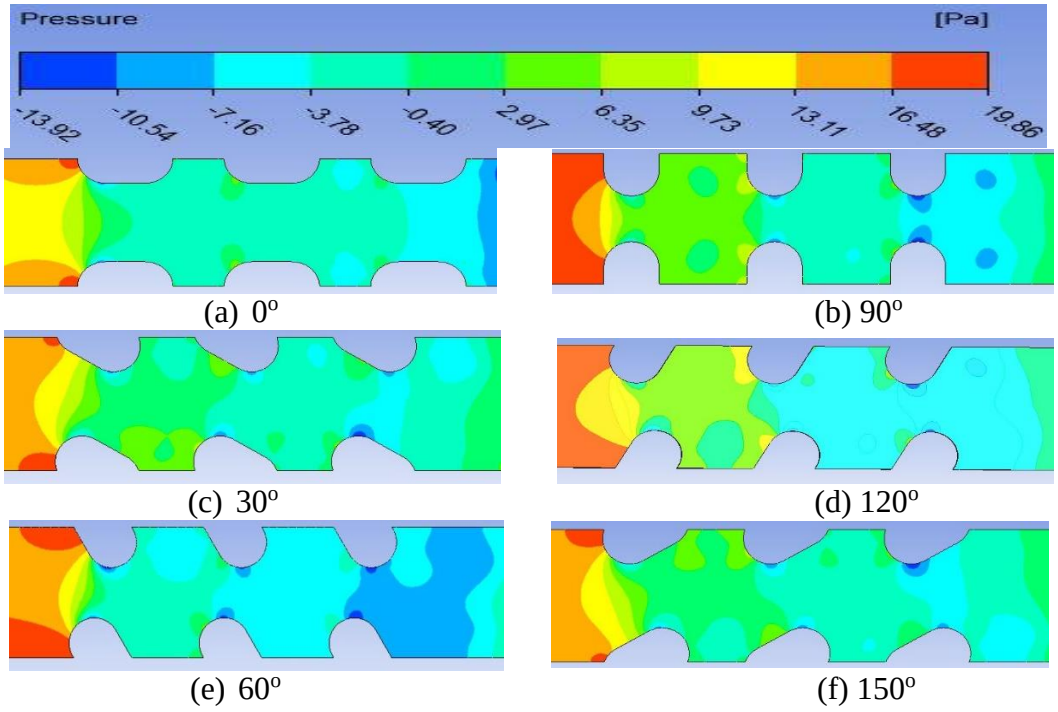

Figure 13. Local pressure distribution for in-line configuration at Re=3500.

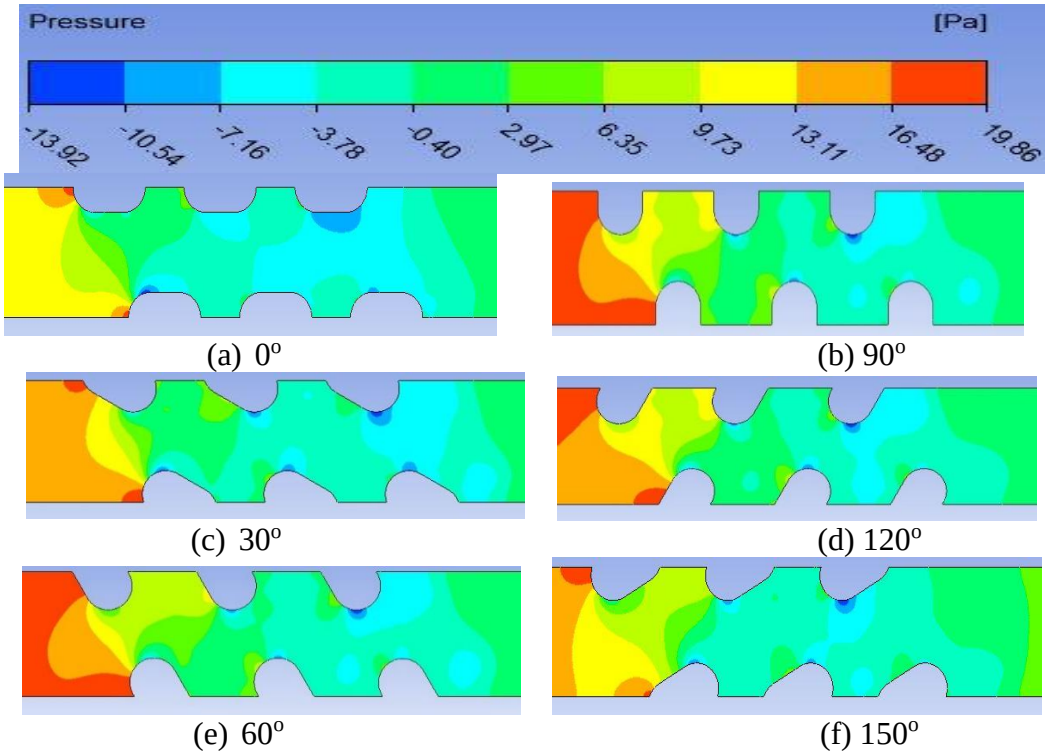

Figure 14. Local pressure distribution for staggered configuration at Re=3500.

Effects of Tube Inclination Angle on the *j* Factor

In fact, the heat transfer enhancement can be obtained using a dimensionless number such as a Nusselt number. Nevertheless, it provides a fractional indication of the overall performance. Thus, to see the overall performance of the HE, area goodness factor (*j*/*f*)

needs to be examined. Figure 15 shows a variation of the area goodness factor with Reynolds number at various tube inclination angles. It can be clearly seen that the *j*/*f* values decreased with the increasing Reynolds number. Therefore, among all the tube inclination angles, 0° had the highest *j*/*f* value for both configurations (in-line and staggered). As expected, the goodness factor for 30° and 150° and for 60° and 120° were close to each other. The lowest goodness factor was obtained at 90° as a result of the high-pressure drop associated with 90º.

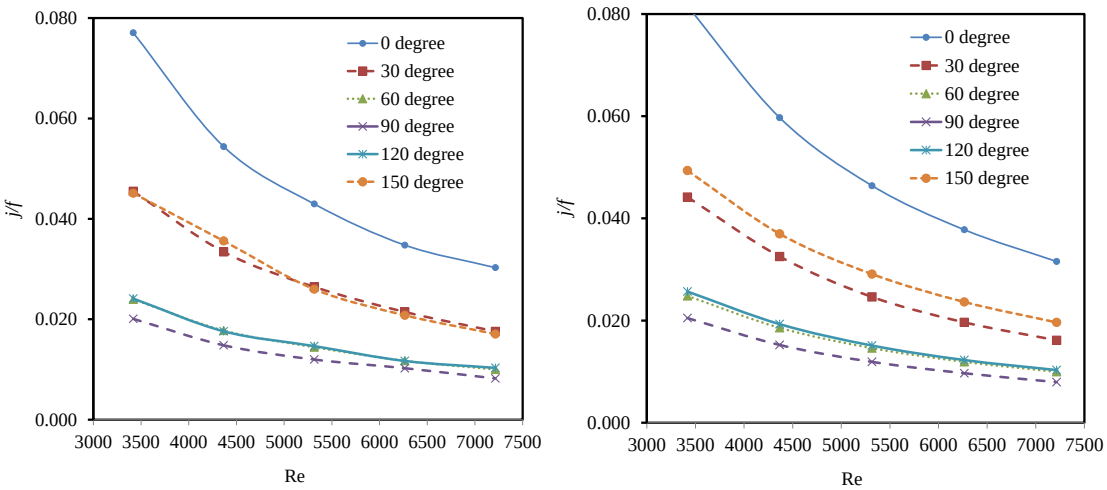

Figure 15. Area goodness factor for different tube inclination angles for (a) in-line and (b) staggered case arrangements.

CONCLUSIONS

In the present paper, two-dimensional numerical simulations were carried out to investigate the heat transfer and pressure drop in finned flat tube HE of different arrangements. The effects of tube inclination angles (0º, 30º, 60º, 90º, 120º, and 150º) on the thermal and hydraulic performances were investigated. The results of the numerical analysis led to the following conclusions. The numerical results confirmed that Nusselt number increased with the increasing flat tube inclination angle. Thus, the maximum and minimum Nusselt numbers were obtained at 90º and 0º, respectively. Similar results were achieved experimentally by other researchers for cross-flow HE without a fin. Flat tubes inclined at 90º provided the highest heat transfer enhancement and pressure drop for both configurations. Therefore, inclining the tubes at 90º is recommended where high heat transfer is required. On the other hand, 0º tube inclination is recommended where pumping power is a crucial issue. Tube inclination angle plays an important role on the heat exchanger performance such as slowing up the separation of the thermal boundary layer, reducing the wake area behind the tube, and thus enhancing the flow mixing behind the tube. As a result, a significant enhancement of heat transfer can occur. The accelerated flow behind the tube cannot merely reduce the wake area and delay the separation of the thermal boundary layer. Nevertheless, it can further impinge the downstream tube which will result in a slight increase of local heat transfer. Comparing the results obtained for in-line and staggered cases, both arrangements provided similar performances in terms of transfer. However, in terms of pressure drop, the staggered arrangement provided low-pressure drop penalty.

ACKNOWLEDGEMENTS

The authors would like to be obliged to Faculty of Mechanical Engineering, University of Malaysia Pahang for providing the necessary support under project no. RDU150375.

REFERENCES

[1] Huang JM, Hsieh WC, Ke XJ, Wang CC. The effects of frost thickness on the heat transfer of finned tube heat exchanger subject to the combined influence of fan types. Applied Thermal Engineering. 2008;28:728-37.

[2] Matos RS, Laursen TA, Vargas JVC, Bejan A. Three-dimensional optimization of staggered finned circular and elliptic tubes in forced convection. International Journal of Thermal Sciences. 2004;43:477-87.

[3] Rao NT, Oumer AN, Jamaludin UK. State-of-the-art on flow and heat transfer characteristics of supercritical CO_2 in various channels. The Journal of supercritical fluids. 2016;116:132-47.

[4] Xie G, Wang Q, Sunden B. Parametric study and multiple correlations on air-side heat transfer and friction characteristics of fin-and-tube heat exchangers with large number of large-diameter tube rows. Applied Thermal Engineering. 2009;29:1-16.

[5] Tahseen TA, Rahman MM, Ishak M. Effect of tube spacing, fin density and Reynolds number on overall heat transfer rate for in-line configuration. International Journal of Automotive and Mechanical Engineering. 2015;12:3065-75.

[6] Tahseen TA, Rahman MM, Ishak M. Heat transfer and pressure drop prediction in an in-line flat tube bundle by radial basis function network. International Journal of Automotive and Mechanical Engineering. 2014;10:2003-15.

[7] Tahseen TA, Rahman MM, Ishak M. An experimental study of air flow and heat transfer over in–line flat tube bank. International Journal of Automotive and Mechanical Engineering. 2014;9:1487-500.

[8] Ishak M, Tahseen TA, Rahman MM. Experimental investigation on heat transfer and pressure drop characteristics of air flow over a staggered flat tube bank in crossflow. International Journal of Automotive and Mechanical Engineering. 2013;7:900-11.

[9] Pongsoi P, Promoppatum P, Pikulkajorn S, Wongwises S. Effect of fin pitches on the air-side performance of L-footed spiral fin-and-tube heat exchangers. International Journal of Heat and Mass Transfer. 2013;59:75-82.

[10] Tang L, Zeng M, Wang Q. Experimental and numerical investigation on air-side performance of fin-and-tube heat exchangers with various fin patterns. Experimental Thermal and Fluid Science. 2009;33:818-27.

[11] Tahseen TA, Ishak M, Rahman MM. A numerical study of forced convection heat transfer over a series of flat tubes between parallel plates. Journal of Mechanical Engineering and Sciences. 2012;3:271-80.

[12] Han H, He YL, Li YS, Wang Y, Wu M. A numerical study on compact enhanced fin-and-tube heat exchangers with oval and circular tube configurations. International Journal of Heat and Mass Transfer. 2013;65:686-95.

[13] Rusdin A. Computation of turbulent flow around a square block with standard and modified k-ε turbulence models. International Journal of Automotive and Mechanical Engineering. 2017;14:3938-53.

[14] Wang L-B, Ke F, Gao S-D, Mei Y. Local and average characteristics of heat/mass transfer over flat tube bank fin with four vortex generators per tube. Journal of Heat Transfer. 2002;124:546-52.
[15] Kim N-H, Kim S-H. Dry and wet air-side performance of a louver-finned heat exchanger having flat tubes. Journal of Mechanical Science and Technology. 2010;24:1553-61.
[16] Tahseen TA, Ishak M, Rahman M. Analysis of laminar forced convection of air for crossflow over two staggered flat tubes. International Journal of Automotive and Mechanical Engineering. 2012;6:755-67.
[17] Gustafsson O, Hellgren H, Stignor CH, Axell M, Larsson K, Teuillieres C. Flat tube heat exchangers–Direct and indirect noise levels in heat pump applications. Applied Thermal Engineering. 2014;66:104-12.
[18] Khoshvaght Aliabadi M, Gholam Samani M, Hormozi F, Haghighi Asl A. 3D-CFD simulation and neural network model for the j and f factors of the wavy fin-and-flat tube heat exchangers. Brazilian Journal of Chemical Engineering. 2011;28:505-20.
[19] Čarija Z, Franković B, Perčić M, Čavrak M. Heat transfer analysis of fin-and-tube heat exchangers with flat and louvered fin geometries. International Journal of Refrigeration. 2014;45:160-7.
[20] Tahseen AT, Ishak M, Rahman MM. A Numerical study of forced convection heat transfer over a series of flat tubes between parallel plates. Journal of Mechanical Engineering and Sciences. 2012;3:271-80.
[21] Nickolas N, Moorthy P, Oumer AN, Ishak M. A review on improving thermal-hydraulic performance of fin-and-tube heat exchangers. IOP Conference Series: Materials Science and Engineering. 2017;257.
[22] Kurnia JC, Sasmito AP. Heat transfer performance of non-circular coiled tubes - Research summary, challenges and directions. International Journal of Automotive and Mechanical Engineering. 2016;13:3710-27.
[23] Nascimento IP, Garcia EC. Heat transfer performance enhancement in compact heat exchangers by using shallow square dimples in flat tubes. Applied Thermal Engineering. 2016;96:659-70.
[24] Duan F, Song K, Li H, Chang L, Zhang Y, Wang L. Numerical study of laminar flow and heat transfer characteristics in the fin side of the intermittent wavy finned flat tube heat exchanger. Applied Thermal Engineering. 2016;103:112-27.
[25] Wais P. Fin-tube heat exchanger performance for different louver angles2014.
[26] Sparrow E, Samie F. Heat transfer and pressure drop results for one-and two-row arrays of finned tubes. International Journal of Heat and Mass Transfer. 1985;28:2247-59.
[27] Dong J, Chen J, Chen Z, Zhang W, Zhou Y. Heat transfer and pressure drop correlations for the multi-louvered fin compact heat exchangers. Energy Conversion and Management. 2007;48:1506-15.
[28] Yang L, Tan H, Du X, Yang Y. Thermal-flow characteristics of the new wave-finned flat tube bundles in air-cooled condensers. International Journal of Thermal Sciences. 2012;53:166-74.
[29] Chu W, Yu P, Ma T, Zeng M, Wang Q. Numerical analysis of plain fin-and-oval-tube heat exchanger with different inlet angles. Chemical Engineering. 2013;35:481-6.

[30] He Y, Han H, Tao W, Zhang Y. Numerical study of heat-transfer enhancement by punched winglet-type vortex generator arrays in fin-and-tube heat exchangers. International Journal of Heat and Mass Transfer. 2012;55:5449-58.
[31] Oumer AN, Mamat O. A study of fiber orientation in short fiber-reinforced composites with simultaneous mold filling and phase change effects. Composites Part B: Engineering. 2012;43:1087-94.
[32] Rao RT, Oumera AN, Jamaludin UK, Hassan I, Firdaus B. Model Validation for Flow and Heat Transfer Characteristics of Supercritical CO_2 in Mini-Channels. ARPN Journal of Engineering and Applied Sciences. 2017;12:4312-7.
[33] Ibrahim TA, Gomaa A. Thermal performance criteria of elliptic tube bundle in crossflow. International Journal of Thermal Sciences. 2009;48:2148-58.
[34] Zukauskas A. Heat transfer from tubes in cross-flow. Advances in heat transfer. 1987;18:87.
[35] Gholami AA, Wahid MA, Mohammed HA. Heat transfer enhancement and pressure drop for fin-and-tube compact heat exchangers with wavy rectangular winglet-type vortex generators. International Communications in Heat and Mass Transfer. 2014;54:132-40.

NOMENCLATURES

C_P specific heat at constant pressure, (J/Kg.K)
D circular tube diameter (mm)
Do tube diameter (mm)
D_h Hydraulic diameter of the tube (m)
f friction factor, dimensionless
h convection heat transfer coefficient, (W/m^2.K)
J Colburn factor, dimensionless
k thermal conductivity of the tube (W/m.k)
L length of the tube (m)
P_l Longitudinal tube pitch, (mm)
P_t Transverse tube pitch, (mm)
q heat flux, (W/m^2)
S fin pitch (mm)
T_{wall} tube wall temperature, (°C)
$Tmean$ mean temperature, (°C)
u_{max} air speed at minimum free flow area (m/s)

Dimensionless group

Nu Nusselt number
Re Reynolds Number
Pr Prandtl number

Subscripts

HEs heat exchangers
max *maximum*

Greek symbols

δ fin thickness (mm)
μ dynamic viscosity, (Kg/m.s)
α tube inclination angle (degree)
ΔP pressure drop (Pa)
ρ density, (Kg/m^3)